

Rowan University

## Rowan Digital Works

---

Faculty Scholarship for the College of Science & Mathematics

College of Science & Mathematics

---

8-10-2016

### Developing hyperpolarized silicon particles for in vivo MRI targeting of ovarian cancer

Nicholas Whiting  
*Rowan University*

Jingzhe Hu  
*University of Texas MD Anderson Cancer Center*

Niki Zacharias  
*University of Texas MD Anderson Cancer Center*

Ganesh Lokesh  
*University of Texas Health Science Center at Houston*

David Volk  
*University of Texas Health Science Center at Houston*

*See next page for additional authors*

Follow this and additional works at: [https://rdw.rowan.edu/csm\\_facpub](https://rdw.rowan.edu/csm_facpub)



Part of the [Biological and Chemical Physics Commons](#), [Materials Science and Engineering Commons](#), and the [Nanoscience and Nanotechnology Commons](#)

---

#### Recommended Citation

Whiting, N., Hu, J., Zacharias, N. M., Ganesh, L. R., Lokesh, D. E., Volk, D. G., ... & Bhattacharya, P. (2016). Developing hyperpolarized silicon particles for in vivo MRI targeting of ovarian cancer. *Journal of Medical Imaging* 3(3), 036001.

This Article is brought to you for free and open access by the College of Science & Mathematics at Rowan Digital Works. It has been accepted for inclusion in Faculty Scholarship for the College of Science & Mathematics by an authorized administrator of Rowan Digital Works.

---

**Authors**

Nicholas Whiting, Jingzhe Hu, Niki Zacharias, Ganesh Lokesh, David Volk, David Menter, Rajesha Rupaimoole, Rebecca Previs, Anil Sood, and Pratip Bhattacharya

# Journal of Medical Imaging

MedicalImaging.SPIEDigitalLibrary.org

## Developing hyperpolarized silicon particles for *in vivo* MRI targeting of ovarian cancer

Nicholas Whiting  
Jingzhe Hu  
Niki M. Zacharias  
Ganesh L. R. Lokesh  
David E. Volk  
David G. Menter  
Rajेशha Rupaimoole  
Rebecca Previs  
Anil K. Sood  
Pratip Bhattacharya

**SPIE.**

Nicholas Whiting, Jingzhe Hu, Niki M. Zacharias, Ganesh L. R. Lokesh, David E. Volk, David G. Menter, Rajेशha Rupaimoole, Rebecca Previs, Anil K. Sood, Pratip Bhattacharya, "Developing hyperpolarized silicon particles for *in vivo* MRI targeting of ovarian cancer," *J. Med. Imag.* **3**(3), 036001 (2016), doi: 10.1117/1.JMI.3.3.036001.

# Developing hyperpolarized silicon particles for *in vivo* MRI targeting of ovarian cancer

Nicholas Whiting,<sup>a,†</sup> Jingzhe Hu,<sup>a,b,†</sup> Niki M. Zacharias,<sup>a</sup> Ganesh L. R. Lokesh,<sup>c</sup> David E. Volk,<sup>c</sup> David G. Menter,<sup>d</sup> Rajesha Rupaimoole,<sup>e</sup> Rebecca Previs,<sup>e</sup> Anil K. Sood,<sup>e,f</sup> and Pratip Bhattacharya<sup>a,\*</sup>

<sup>a</sup>University of Texas MD Anderson Cancer Center, Department of Cancer Systems Imaging, 1515 Holcombe Boulevard, Houston, Texas 77030, United States

<sup>b</sup>Rice University, Department of Bioengineering, 6100 Main Street, Houston, Texas 77005-1892, United States

<sup>c</sup>University of Texas Health Science Center at Houston, Department of NanoMedicine and Biomedical Engineering and the Institute of Molecular Medicine, 7000 Fannin, Houston, Texas 77030, United States

<sup>d</sup>University of Texas MD Anderson Cancer Center, Department of Gastrointestinal Medical Oncology, 1515 Holcombe Boulevard, Houston, Texas 77030, United States

<sup>e</sup>University of Texas MD Anderson Cancer Center, Department of Gynecologic Oncology and Reproductive Medicine, 1515 Holcombe Boulevard, Houston, Texas 77030, United States

<sup>f</sup>University of Texas MD Anderson Cancer Center, Center for RNA Interference and Non-Coding RNA, 1515 Holcombe Boulevard, Houston, Texas 77030, United States

**Abstract.** Silicon-based nanoparticles are ideally suited for use as biomedical imaging agents due to their biocompatibility, biodegradability, and simple surface chemistry that facilitates drug loading and targeting. A method of hyperpolarizing silicon particles using dynamic nuclear polarization, which increases magnetic resonance imaging signals by several orders-of-magnitude through enhanced nuclear spin alignment, has recently been developed to allow silicon particles to function as contrast agents for *in vivo* magnetic resonance imaging. The enhanced spin polarization of silicon lasts significantly longer than other hyperpolarized agents (tens of minutes, whereas <1 min for other species at room temperature), allowing a wide range of potential applications. We report our recent characterizations of hyperpolarized silicon particles, with the ultimate goal of targeted, noninvasive, and nonradioactive molecular imaging of various cancer systems. A variety of particle sizes (20 nm to 2  $\mu$ m) were found to have hyperpolarized relaxation times ranging from  $\sim$ 10 to 50 min. The addition of various functional groups to the particle surface had no effect on the hyperpolarization buildup or decay rates and allowed *in vivo* imaging over long time scales. Additional *in vivo* studies examined a variety of particle administration routes in mice, including intraperitoneal injection, rectal enema, and oral gavage. © 2016 Society of Photo-Optical Instrumentation Engineers (SPIE) [DOI: 10.1117/1.JMI.3.3.036001]

Keywords: hyperpolarization; magnetic resonance imaging; silicon nanoparticles; molecular imaging.

Paper 16048PR received Mar. 25, 2016; accepted for publication Jul. 18, 2016; published online Aug. 10, 2016.

## 1 Introduction

### 1.1 Silicon Particles

Shaped particles consisting of elemental silicon or silicon dioxide (silica) in the nanometer- to micrometer-size scale are receiving heightened interest for medical applications, including drug delivery and sensing,<sup>1</sup> due to their low cost and lack of toxicity for both the initial particles and their biodegradable downstream products.<sup>2</sup> Fluorescently tagged silicon particles have been used to track living cells after uptake into the cytoplasm<sup>3</sup> while naturally luminescent silicon nanoparticles (<10 nm) have been applied in tracking pancreatic cancer cells *in vitro*.<sup>4</sup> Furthermore, commercially available particles are also undergoing clinical trials for slow release drug delivery in the treatment of pancreatic cancer.<sup>5</sup> Because <sup>29</sup>Si (nuclear spin: 1/2; natural abundance:  $\sim$ 4.6%) is detectable using magnetic resonance imaging (MRI) or spectroscopy (MRS), developing silicon-based nanomaterials for MR studies may prove beneficial.

<sup>29</sup>Si MRI provides positive-contrast, background-free signals that are within the frequency range of most broadband MR scanners that are capable of detecting <sup>13</sup>C signals. Silicon particles ranging in size, porosity, purity, and crystallinity are commercially available and cost-effective, and the field of silicon nanomaterials can benefit from developmental interests from the semiconductor industry. The simple surface chemistry of silicon particles is amenable to the addition of targeting agents and therapeutic drugs—furthering their application to the biomedical community—and small particles (<100 nm) have increased circulation times in the vasculature (compared to larger particles, which are more likely to be trapped by the reticuloendothelial system).<sup>6</sup>

### 1.2 Hyperpolarized Magnetic Resonance

MRI and MRS measure the interactions of nuclear spins with radiofrequency waves inside of a strong magnetic field. Due to the small energetic differences in nuclear spin levels compared to thermal energy, and the fact that the spins populating these energy levels are oppositely aligned, the majority of the

\*Address all correspondence to: Pratip Bhattacharya, E-mail: [pkbhattacharya@mdanderson.org](mailto:pkbhattacharya@mdanderson.org)

<sup>†</sup>These authors contributed equally to this work.

available magnetization is cancelled, leaving only a miniscule number of nuclear spins to contribute to MR signals. This population difference, termed “polarization” ( $P$ ), is typically on the order of  $10^{-5}$  to  $10^{-6}$  at thermal equilibrium, and it is the primary reason for the relatively low detection sensitivity of MR-based techniques. Clinical MR studies focus on  $^1\text{H}$  spins because they possess the highest gyromagnetic ratio ( $\gamma$ )—providing more signal per spin, near-unity isotopic abundance, and are highly prevalent *in vivo*. Aside from  $^{19}\text{F}$ ,<sup>7</sup> most other MR-active species (including  $^{29}\text{Si}$ ) have orders-of-magnitude lower detection sensitivity compared to  $^1\text{H}$  due to lower  $\gamma$  and isotopic abundance, limiting their feasibility for study in clinical settings. One way to overcome the sensitivity challenge is through “hyperpolarization” (HP), which refers to a collection of methods that temporarily boost MR signal intensities by redistributing the population of nuclear spins so that most occupy the same energy level—allowing the spins to constructively contribute to enhancing MR signals as opposed to destructively canceling each other’s effect. This process typically uses magnetic fields, low temperatures, and/or electromagnetic radiation to manipulate the nuclear spin population. Most hyperpolarization methods will highly spin-polarize an electron bath to near unity, then transfer this spin polarization to nearby nuclear spins through dipolar interactions. The result is an increase in detection sensitivity by four to five orders-of-magnitude, allowing the study of “nonconventional” nuclei for molecular and metabolic imaging studies. Some of these include monitoring the metabolic conversion of HP  $^{13}\text{C}$ -pyruvate to lactate and alanine to probe cellular metabolic pathways<sup>8</sup> in the field of cancer detection,<sup>9</sup> as well as lung space imaging using HP  $^3\text{He}$  and  $^{129}\text{Xe}$  in patients with chronic obstructive pulmonary disease or asthma.<sup>10</sup>

### 1.3 Solid-State Dynamic Nuclear Polarization of Silicon

A method of hyperpolarizing silicon micro- and nanoparticles<sup>11</sup> using solid-state dynamic nuclear polarization (DNP) has recently been developed<sup>12</sup> and shown viable for *in vivo* imaging studies<sup>13</sup> in mice. In this method, low temperatures (<4 K) and high magnetic fields ( $\sim 3$  T) are used to spin-polarize an ensemble of electrons. Then, this polarization is transferred to nearby nuclei through microwave-mediated dipolar spin-flips; this process takes place on the surface of the silicon particles, which contain naturally occurring oxidation defects. Because of this, the silicon particles do not require the addition of an exogenous radical source of free electrons,<sup>14</sup> which is needed for most other nuclear species polarized by conventional DNP (such as  $^{13}\text{C}$ -labeled metabolites). The polarization is then spread into the core of the particle via nuclear spin diffusion.<sup>12</sup> Because the core of the particle is protected from exposure to depolarizing paramagnetic agents, the enhanced polarization is retained for tens of minutes—significantly longer than most other hyperpolarized species, which typically lose their signal enhancement in tens of seconds<sup>15</sup> *in vivo*. This increased hyperpolarized relaxation time (HP  $T_1$ ) holds true even under physiological conditions and creates an MR imaging window of at least 1 h, allowing the particles (once injected) the chance to transit to the physiological site of interest in a relevant timescale for targeted molecular imaging. Furthermore, the silicon particles, hyperpolarization process, and MRI/MRS in general are nontoxic and nonradioactive.

### 1.4 Purpose

We have previously demonstrated proof-of-concept *in vivo* imaging of unfunctionalized silicon microparticles in mouse models,<sup>13</sup> as well as for MRI-guided angiocatheter tracking.<sup>16</sup> Additional work by other researchers has focused on fundamental studies<sup>11,12,14,15</sup> of the hyperpolarization process in silicon particles. For this work, our goal was to transition into a new regime of molecular imaging by functionalizing the silicon particle surface with a thioaptamer that targets ovarian tumors. We then studied the effects of particle size (20 nm to  $2\ \mu\text{m}$ ) and surface functionalization on the hyperpolarization dynamics. A variety of relevant particle administration routes in mouse models were also examined to deduce the ideal method to introduce hyperpolarized silicon particles into mice with different cancer models. Successful demonstration of long-lasting hyperpolarized  $^{29}\text{Si}$  signal from functionalized particles *in vivo* is a significant step forward in their development as targeted MR imaging agents.

## 2 Methods

### 2.1 Silicon Particles

Different commercially sourced silicon powders were either used as received (‘unfunctionalized’ or ‘bare’), or were coated in (3-aminopropyl)triethoxysilane (APTES), then cross-linked with either polyethylene glycol (PEG)—for improved hydrophilicity and biocompatibility, or an oligonucleotide aptamer—for targeting of a specific cancer system (Sec. 3.2). The average mean diameter of the bare particles ranged in size from 20 nm to  $2\ \mu\text{m}$ ; the smaller nanoscale particles were mostly monocrystalline, while larger microparticles were polycrystalline/amorphous. For each silicon particle sample,  $\sim 50$  to 100 mg of dry silicon powder was packed into a small Teflon sample tube (3.2 mm ID  $\times$  2 cm length) that is normally used as an insert for electron spin resonance (ESR) experiments; these tubes are microwave-invisible and withstand the cryogenic temperatures of DNP.

### 2.2 Particle Functionalization Protocol

**APTES coating:** SiNPs are added to 70% ethanol aqueous solution acidified to pH 2.5 (50 mg particles and 14 ml of solution). Particles are sonicated for 5 min and then APTES (Sigma-Aldrich, CAS 919-30-2) is added to the solution to generate a 150-mM APTES solution. Solution is shaken on a mechanical rotator overnight. Particles are isolated by centrifugation (5 min, 4000g) and the supernatant is removed. Particles are then washed three times with ethanol, and then isolated by centrifugation. With the final wash, particles in solution are aliquoted into preweighed Eppendorf tubes, tubes are centrifuged, supernatant removed, and the tubes are placed on vacuum centrifuge to remove any remaining ethanol. Ninhydrin tests of particles were positive for amines after APTES coating.

**Aptamer coupling:** For a 200-mg SiNP reaction, 420 mg of 1-ethyl-3-(3-dimethylaminopropyl)carbodiimide (EDC, Sigma-Aldrich, CAS 1892-57-5) was dissolved in 2.1 ml of 50 mM citrate buffer (pH 5.5) vortexed and put on ice. An amount of 420 mg of *N*-hydroxysuccinimide (NHS, Sigma-Aldrich, CAS 6066-82-6) was dissolved in 2 ml of citrate buffer, vortexed, and put on ice. Reagent solutions were made fresh for each coupling. Combined: a solution of thioaptamer (that targets the E-Selectin protein) that was synthetically generated to have

a carboxylic acid tail (169  $\mu\text{M}$ , 1 ml), 250  $\mu\text{l}$  EDC solution, and 250  $\mu\text{l}$  NHS solution. Reaction was allowed to proceed for 15 min at room temperature, and then another 250  $\mu\text{l}$  of both EDC and NHS solution was added. Reaction was allowed to go for another 15 min at room temperature. During the NHS-ester formation reaction, 200 mg of SiNPs were dissolved in 4 ml of borate solution (40 mM, pH 9.25) and sonicated for 5 min. After sonication, the fully activated aptamer solution was added to the particles, and the reaction was allowed to rotate on a mechanical rotator for 4 h at room temperature. Solution was then centrifuged (10 min, 4000g), supernatant removed, and the particles washed three times with 3 ml of ethanol. After washes, particles were centrifuged down, supernatant removed, and particles were stored moist at 4°C.

### 2.3 Solid-State Dynamic Nuclear Polarization

The sample tube is push-fit onto the end of a G10 fiberglass rod and inserted into the (laboratory-built) solid-state DNP device (Fig. 1), which consists of a superconducting magnet ( $\sim 2.9$  T), helium flow cryostat ( $\sim 3$  K), and microwave source ( $\sim 100$  mW) that was frequency-modulated from 80.83 to 80.90 GHz to accommodate the relatively wide silicon ESR spectrum. The microwaves were directed to the sample tube using a waveguide and slot antenna. Inside the cryostat, the sample resides within an *in situ* NMR coil, allowing quality assurance using a miniature NMR spectrometer, and next to a resistance thermocouple (for temperature monitoring). During DNP, the buildup of  $^{29}\text{Si}$  signal was monitored by applying a single pulse with a small tipping angle at set time points during the buildup. After sufficient polarization time (1 to 17 h), the sample tube was quickly removed from the cryostat, warmed to room temperature, and transported to the MRI scanner suite for imaging studies ( $T_{\text{transport}} < 1$  min).

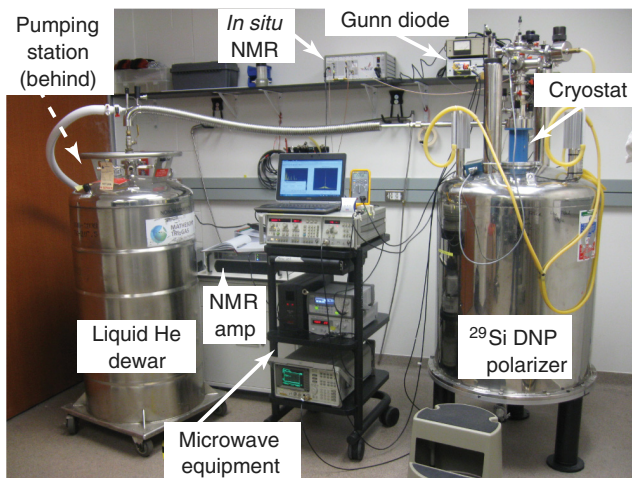


**Fig. 1** Labeled picture of laboratory-constructed solid-state DNP device for  $^{29}\text{Si}$  hyperpolarization. The magnetic field is supplied via superconducting magnet, while a liquid helium flow cryostat allows the sample to be held at cryogenic temperatures. The Gunn diode provides microwaves to transfer polarization from electrons to nearby nuclei, and the on-board NMR system allows the buildup of  $^{29}\text{Si}$  hyperpolarization to be monitored in real time for dynamics studies and quality control.

### 2.4 Imaging Protocol

All imaging experiments were performed on a 7 T horizontal-bore small animal MRI scanner using either a dual-tuned  $^1\text{H}/^{29}\text{Si}$  litz coil for coregistered imaging (35 mm ID; homogeneous rf region  $\sim 52$  mm along  $z$ -axis; Doty Scientific) or a dual-coil setup consisting of a laboratory-constructed  $^{29}\text{Si}$  surface coil (30 mm) and a commercial  $^1\text{H}$  volume coil (35 mm ID; Bruker). A small aliquot ( $\sim 1.5$  ml) of silicon oil was used for  $^1\text{H}$  and  $^{29}\text{Si}$  sequence calibration purposes; achievable  $^{29}\text{Si}$  nuclear spin polarization values were typically on the order of  $\sim 1\%$ . Spectroscopy (both in the DNP device and the 7 T MRI scanner) was performed using a simple pulse/acquire sequence. Imaging studies of solid-state particles, dissolved particles in phantoms, and *in vivo* mouse models used a rapid acquisition with refocused echoes (RARE) sequence. Image reconstruction and postprocessing were performed in MATLAB<sup>®</sup>. For dissolution studies, particles were removed from the sample tube, suspended in warmed phosphate-buffered saline (PBS), and then administered to the phantom or mouse model via syringe.

### 2.5 Animal Handling

All animal studies were performed in accordance with the UT MD Anderson Cancer Center Institutional Animal Care and Use Committee (IACUC). Mice were placed on an MR-compatible warming sled and anesthetized with 2% isoflurane (in 0.75 l/min oxygen) administered via nose cone. Following hyperpolarization, silicon particles were dissolved/suspended in PBS and administered to the mice using various delivery mechanisms, including intraperitoneal injection, oral gavage, tail vein injection, intratumoral injection, or administered via the rectum (e.g., enema). Injected mice showed no ill effects that could be attributed to the presence of the silicon particles in their system. Mouse models used were (1) normal nude mice (i.e., control), along with two cohorts of nude mice that received an orthotopic injection of (2) *HeyA8* or (3) *SKOV3* ovarian cancer cell lines. Once the tumor burden became sufficient to be physically palpable, the mice were used for imaging studies.

## 3 Results and Discussion

### 3.1 Effects of Particle Size

A number of different silicon particle sizes were evaluated, ranging from 20 nm to 2  $\mu\text{m}$  average mean diameter. While the larger microparticles provided greatly enhanced  $^{29}\text{Si}$  NMR signals, the smaller nanoscale particles produced relatively smaller signal enhancements. However, even with diminished hyperpolarization capacity in Si nanoparticles, significant enhancements were still achieved. Figure 2 compares hyperpolarized  $^{29}\text{Si}$  NMR spectra taken during DNP versus what was available with the same sample without DNP (i.e., thermal polarization; inset)—showing an enhancement in  $^{29}\text{Si}$  signal by several orders of magnitude. Additionally, the hyperpolarized signal was attained in a single scan ( $< 1$  s), while the thermal sample required averaging 16,000 transients to separate the signal from the noise—taking around 4 days to complete.

The time needed to reach steady-state polarization was dependent on particle size, due to the nuclear spin diffusion mechanism that spreads the hyperpolarization from the surface to the core of the particle. Smaller nanoparticles ( $< 100$  nm) only required  $\sim 1$  h of DNP time to reach steady-state polarization

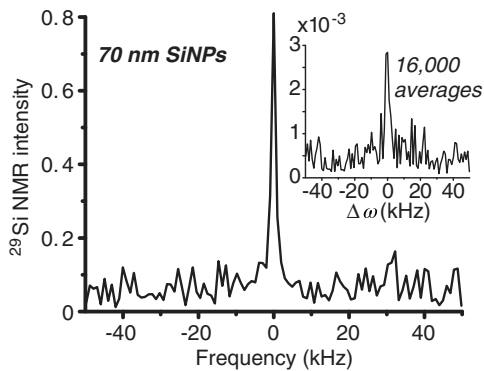


**Fig. 2**  $^{29}\text{Si}$  NMR spectra of 70 nm silicon nanoparticles (56 mg) after 105 min of DNP, showing the ability to hyperpolarize silicon particles on the nanoscale (single acquisition). Inset:  $^{29}\text{Si}$  NMR spectra of the same sample acquired under thermal equilibrium (room temperature, without DNP); signal was still  $\sim 300\times$  less than hyperpolarized sample, even with 16,000 signal averages (100  $\mu\text{s}$  pulse for both instances).

levels, while larger microparticles needed more than 10 h to achieve steady-state polarization (Fig. 3). Furthermore, a dependence on the overall  $^{29}\text{Si}$  NMR signal intensity versus particle size was observed. This dependence was likely due to: (a) differences in the number and position of electronic defects as a function of particle size and crystallinity, and/or (b) differences in surface-to-volume ratio between particle sizes. Note that polarization is quickly depleted on the surface, while spins in the particle core are relatively protected, thereby differentially depleting  $^{29}\text{Si}$  polarization in smaller particles to a greater extent.<sup>17</sup>

Because of this significant difference in attainable signal intensities across particle sizes (factor of  $\sim 25\times$ , adjusted for sample mass), only larger microparticles (2  $\mu\text{m}$ ) were studied for *in vivo* applications at this time. Current studies are focused on altering the surface defects of smaller nanoparticles (<100 nm) using heat and chemical treatments in order to improve DNP efficiency. Alternatively, a ball mill was applied in an attempt to break apart the larger microparticles; however, preliminary studies were hindered by contamination from the ball mill jar material (stainless steel). Future studies will examine the effects

**Table 1**  $^{29}\text{Si}$  polarization decay times (HP  $T_1$ ) for different silicon nanoparticle (SiNP) sizes, surface chemistries, and time spent in the DNP device. Particles of 2  $\mu\text{m}$  size are shown with normal surface chemistry, as well as the addition of PEG and an ESTA-1 agent that targets ovarian cancer.

$^{29}\text{Si}$  hyperpolarization decay times

SiNP size	HP $T_1$	DNP time
20 nm	$\sim 10$ min	$\sim 80$ min
30 nm	$\sim 17$ min	$\sim 120$ min
70 nm	$\sim 16$ min	$\sim 60$ min
2000 nm	$\sim 62$ min	$\sim 300$ min
2000-nm PEGylated	$\sim 55$ min	$\sim 330$ min
2000-nm ESTA-1	$\sim 56$ min	$\sim 300$ min

of using nonferrous jars and balls; even without contamination, it remains unclear whether the resulting particles will retain a favorable consistency (and position) of electronic defects, as well as crystallinity, and with a relevant size/shape distribution.

Because the primary means of depolarization (hence, signal loss) is through nuclear spin diffusion from the core back to the surface (provided the lack of internal impurities), the hyperpolarization relaxation time also depends on the particle size, with smaller particles losing the signal enhancement at a faster rate than larger particles due to the decreased distance from the surface to the core and higher surface-to-volume ratio (Table 1). In spite of this, even small particles (<100 nm) retain hyperpolarized signals for  $\geq 10$  min, which is still an order-of-magnitude greater than most other hyperpolarized contrast agents *in vivo*.

### 3.2 Effects of Surface Chemistry

While bare, unfunctionalized silicon microparticles [Fig. 4(a)] showed promise for hyperpolarization studies, modifications

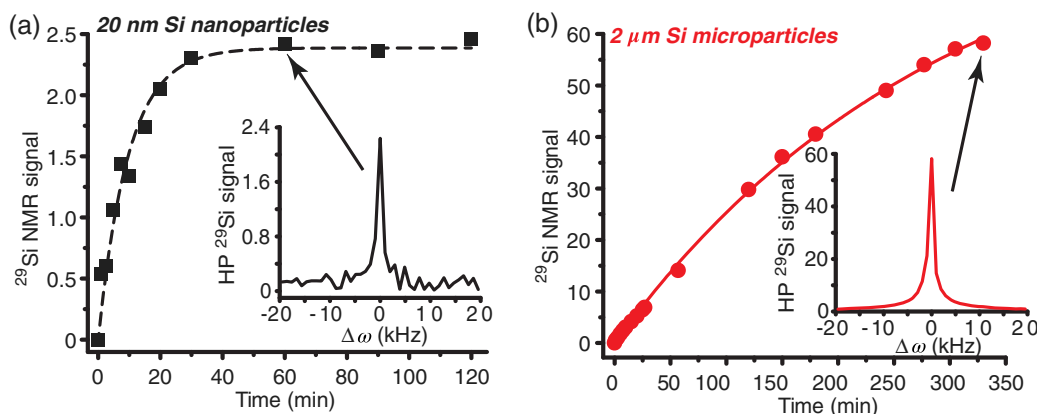


**Fig. 3** Hyperpolarized  $^{29}\text{Si}$  polarization buildup curves for (a) 20 nm and (b) 2  $\mu\text{m}$  silicon particles. Silicon microparticles provide  $\sim 25\times$  more  $^{29}\text{Si}$  NMR signal than the nanoscale particles, but take significantly longer to reach steady-state polarization. Insets: example NMR spectra at relevant time points [(a) 60 min and (b) 330 min]. Data were collected in real time during DNP process and using on-board NMR system and a pulse/acquire sequence (100  $\mu\text{s}$  pulse duration; 24.4 MHz). All data were normalized to sample mass.

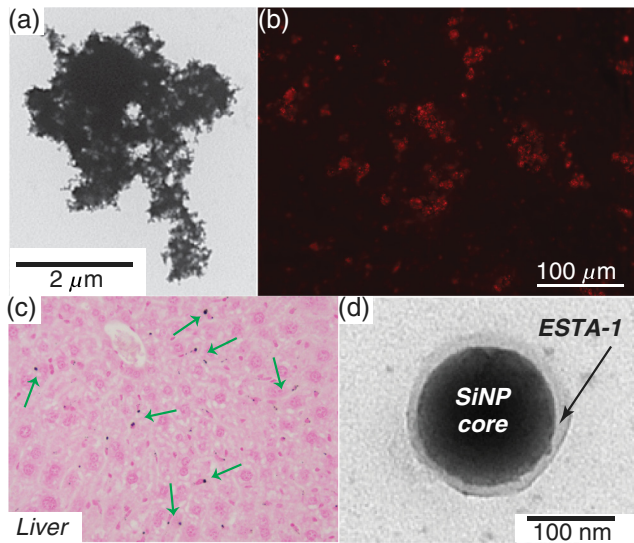


**Fig. 4** Microscopy images of silicon particles. (a) Representative tunneling electron micrograph (TEM) of standard silicon microparticle. (b) Optical microscopy of silicon microparticles that have been functionalized with ESTA-1 and Cy3 dye, showing successful coupling of functional groups to silicon particles. (c) Nuclear fast red staining of cells from an excised mouse liver—silicon microparticles previously administered to the alive mouse via intraperitoneal injection 1 week prior; green arrows denote some of the silicon microparticles (black dots). (d) TEM of a  $\sim 70$  nm silicon nanoparticle functionalized with ESTA-1, appearing as the translucent layer on the particle surface.

to the surface chemistry would greatly increase their utility for selective targeting and imaging *in vivo*. Studies were performed to further develop silicon particles as targeted molecular imaging agents by adding functional groups to the particles' surface and testing the effects of these altered surface chemistries on the hyperpolarization dynamics. Particles were functionalized with PEG to improve hydrophilicity and biocompatibility; indeed, the PEGylated particles exhibited improved dissolution

characteristics when compared to bare silicon particles. Intraperitoneal injection of PEGylated particles into a normal nude mouse, followed by  $\sim 1$  week of wait time, showed particle accumulation primarily in the liver [Fig. 4(c)] and spleen, with slight accumulation in the lung, ovary/oviduct, and bone marrow. The prevalence of particle accumulation in the liver and spleen was consistent with the expectation that larger particles would be taken up by the reticuloendothelial system.

E-selectin thioaptamer (ESTA-1), a monothiophosphate-modified oligonucleotide aptamer<sup>18,19</sup> that binds to E-selectin—a glycoprotein that is overexpressed on the endothelial cell surface of certain ovarian cancer tissue—was also conjugated to the silicon particles [Figs. 4(b) and 4(d)] for molecular targeting of ovarian cancer. E-selectin is not present in significant quantities in normal ovarian tissue, making it a potentially useful biomarker for ovarian cancer. On their own (unconjugated to the silicon particles), the thioaptamers<sup>20</sup> bind to E-selectin with nanomolar affinity and are minimally cross-reactive with other selectins. When conjugated to particles, ESTA-1 has been demonstrated as safe<sup>21</sup> and shown to target breast cancer metastasis.<sup>22,23</sup> They also bind to cultured endothelial cells and tumor-associated vasculature in murine and human carcinomas. In addition to the high levels of affinity and specificity, thioaptamers are easily synthesized and conjugated to particles, as well as remaining biocompatible and resistant to nuclease.

These ESTA-1 functionalized particles were tagged with a fluorescent dye (Cy3) to allow for future cross-correlation between MRI and optical imaging studies. Importantly, because <sup>29</sup>Si DNP uses endogenous electronic defects,<sup>14</sup> the addition of these functional groups to the particle surface did not diminish the capacity for hyperpolarization buildup or relaxation rates (Fig. 5). This ability to hyperpolarize aptamer-functionalized silicon particles was an important step in their progression as targeted imaging agents. Ongoing and future studies will focus on administering these ESTA-1 silicon particles into orthotopic ovarian cancer mouse models to test their ability to function as targeted imaging agents (Sec. 3.5).

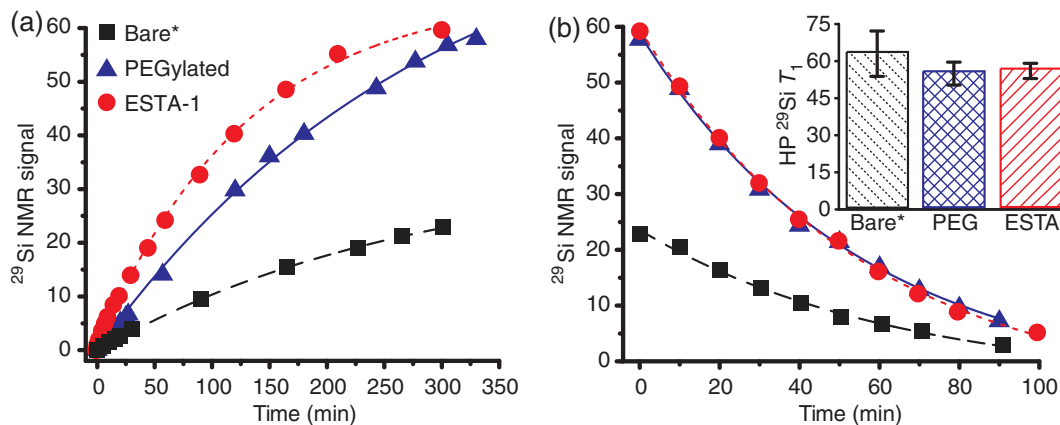


**Fig. 5** Plots of hyperpolarized <sup>29</sup>Si NMR signal (normalized by sample mass) buildup (a) and decay (b) for samples with different surface chemistries: “Bare” particles (black squares), as well as those with added PEG (blue triangles) and ESTA-1 (red circles) functionalities coupled to the particle surface. Inset: HP  $T_1$  values for the three particle types, calculated from decay rates in (b). \*Bare data taken 2 months after other data; during that time the Q of the NMR coil drifted, contributing to the lower overall signal of the “Bare” data (but without affecting the buildup/decay rates). Hyperpolarization buildup and decay rates very similar across datasets; slight increase in buildup rate for ESTA-1 particles and slightly longer  $T_1$  for bare particles noticed.

### 3.3 Initial Imaging Studies

Following DNP, the sample can be efficiently transferred to the small animal MRI scanner while retaining sufficient hyperpolarized signal to allow  $^{29}\text{Si}$  imaging experiments. Compared to previous studies<sup>13</sup> at a different location using the same experimental parameters, the 7-T scanner in this study provides nearly an order-of-magnitude improvement in signal-to-noise ratio due to newer hardware and improved electromagnetic shielding properties. Because the benefits of the hyperpolarization process are field-independent, the increase in field strength between studies ( $4.7 \rightarrow 7$  T) was largely inconsequential for  $^{29}\text{Si}$  MRI (but improved  $^1\text{H}$  anatomical imaging). Initial imaging scans using the silicon particles in their sample tube as a phantom reveal that the signal was still observable 30 min after completion of the DNP process (Fig. 6). Most other biomedically relevant HP imaging agents have much shorter hyperpolarized relaxation times under ambient conditions (e.g., HP  $T_1$  of  $^{13}\text{C}$ -pyruvate  $\sim 1$  min).<sup>8</sup> This longer relaxation time will allow the silicon particles to accumulate at their targeted site *in vivo* in a timeframe relevant for molecular imaging.

### 3.4 Silicon Particle Administration Routes

Following the successful phantom imaging, we performed proof-of-concept studies in mouse models to demonstrate the long-lasting hyperpolarized  $^{29}\text{Si}$  signal. In addition to targeting ovarian cancer, hyperpolarized silicon particles can be considered as a “platform technology,” where different disease systems can be interrogated in real time by adding a variety of targeting groups to the particle surface. Because different cancer systems arise (and are orthotopically modeled) at dissimilar locations throughout the body, and the optimal delivery of the targeted particles is needed to maximize the chances of success, a variety of particle dissolution/suspension and administration methods were tested in mouse models. It was found that the (manual) dissolution process works optimally in the fringe field of the 7-T MRI scanner, where the field is strong (compared to Earth’s field) and the chance of hyperpolarization-depleting zero-field crossing is minimized. The particles were administered to the mouse models in a variety of ways; these include injecting into the intraperitoneal (IP) cavity, tail vein, administering to the large intestines via the rectum (i.e., enema), as well as through oral gavage.

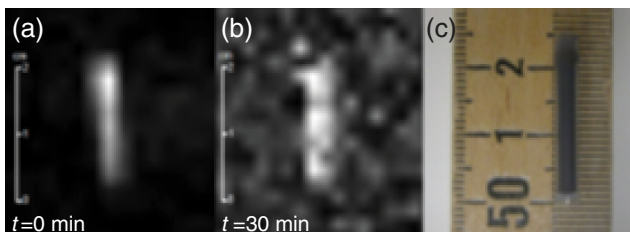


**Fig. 6** Initial  $^{29}\text{Si}$  MR image of silicon particles packed inside sample tube. (a) Image acquired using a 10 deg RARE sequence immediately after 4 h of DNP. (b) Image acquired using a 90 deg RARE sequence 30 min after (a). (c) Photo of silicon particles in sample tube/phantom (particle region: 2 cm long; 3.2 mm internal diameter). 137 mg of unfunctionalized  $2\ \mu\text{m}$  silicon particles (dry powder) were used for this study. TR/TE: 1 s/1.761 ms; RARE factor = 32; imaging resolution = 2 mm; single scan acquisition (1 s).

Tail vein injection, which is the most common method of intravascular administration of MR contrast agents to mouse models, could not be used for the  $2\text{-}\mu\text{m}$  sized particles due to their large size and relative insolubility, despite PEGylation. Injected particles would travel  $\sim 1$  cm up the tail vein before stopping due to a blockage or clog. Also, the viscosity and propensity for aggregation of the microparticle suspension requires the use of a larger needle, which is not conducive to tail vein injections. Future use of smaller nanoscale silicon particles may enable the reevaluation of this administration route for *in vivo* studies.

The alternative administration routes were more successful, and *in vivo* hyperpolarized  $^{29}\text{Si}$  imaging were achieved using PEGylated silicon microparticles. Oral gavage, which can be used to study diseases of the upper gastrointestinal tract, was difficult to administer in a timely fashion using a soft plastic oral gavage needle (due to proximity to MRI scanner) and while keeping the mouse stationed on the sled. However, we were able to acquire  $^{29}\text{Si}$  images of the particles inside the stomach using this method [Fig. 7(a)]. Injections into the rectum (via the anus), to study diseases of the large intestines, were achieved

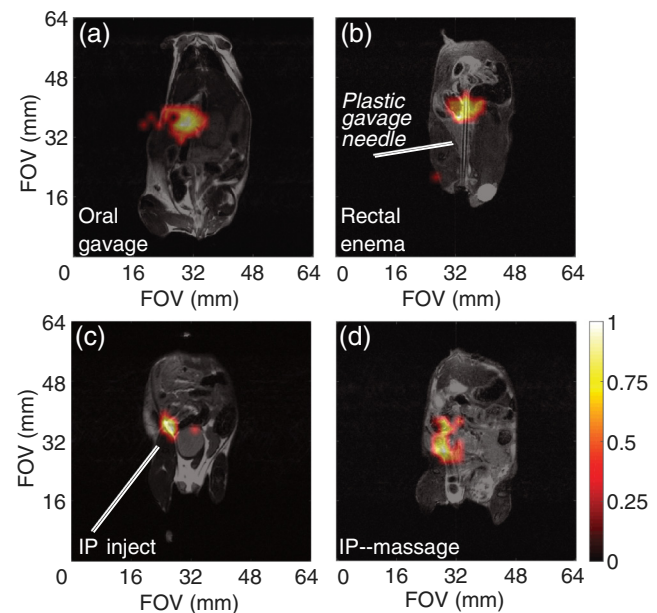


**Fig. 7** *In vivo*  $^{29}\text{Si}$  MRI for  $2\ \mu\text{m}$  silicon particles. (a) Administration of  $\sim 135$  mg of PEGylated silicon particles (in  $300\ \mu\text{l}$  PBS) into a normal mouse via oral gavage, followed by a 5-min wait prior to imaging. (b) Administration of  $\sim 135$  mg of PEGylated silicon particles (in 1 ml PBS) via injection through the rectum of a normal mouse using a soft plastic gavage needle (3.8 mm diameter), followed by a 5-min wait prior to imaging. (c) Administration of  $\sim 100$  mg of PEGylated silicon particles (in  $300\ \mu\text{l}$  PBS) via intraperitoneal injection into a normal mouse, followed by a 30-min wait prior to imaging; gravitational settling is noted at the injection site. (d) Administration of  $\sim 135$  mg of ESTA-1 functionalized silicon particles (in  $600\ \mu\text{l}$  PBS) into a SKOV3 mouse via intraperitoneal injection, followed by physical manipulation of the mouse’s abdomen to help distribute the particles, then a 10-min wait prior to imaging.  $^{29}\text{Si}$  imaging scans (color): 90 deg RARE imaging sequence, TR/TE: 59.9/1.8 ms, FOV:  $64 \times 64$  mm, resolution: 2 mm; single scan acquisition (scan time  $\sim 60$  ms), processed with 35% threshold to filter background. Coregistered with  $^1\text{H}$  imaging scans (grayscale): 90 deg RARE imaging sequence, coronal plane, TR/TE: 1800/9.5 ms, FOV:  $64 \times 64$  mm; resolution: 0.25 mm; three averages (scan time  $\sim 3$  min).

through insertion of a soft, flexible applicator needle or small diameter ( $\sim 1/8$  in.) rubber tube [Fig. 7(b)]. This method kept the particle concentration per voxel high (as the particles are contained in the defined volume of the intestines), leading to increased  $^{29}\text{Si}$  signal. The success of this method was improved when it was used after the administration of a saline enema (Fleet) at least 30 min prior to particle insertion. Additional gains may be achieved when implementing dietary restrictions and laxatives the night prior to the scan. Fecal blockages can be problematic with this administration route, but silicon particles delivered in this fashion have been imaged in the large intestines from the rectum to the cecum. Ongoing work includes improving multislice  $^{29}\text{Si}$  imaging sequences that will help differentiate the three-dimensional folding of the intestinal tract.

IP injections of hyperpolarized microparticles [Fig. 7(c)], which can be used for targeting orthotopic ovarian cancer, displayed sufficient  $^{29}\text{Si}$  signal postinjection. However, the majority of the  $^{29}\text{Si}$  signal was concentrated at the injection site, meaning that the large microparticles did not disperse throughout the cavity. Postinjection physical manipulation (e.g., massage) of the mouse's abdomen [Fig. 7(d)] resulted in spatial movement of the  $^{29}\text{Si}$  signal, but it is not considered active targeting. It is likely that the large size of the microparticles prevents them from actively transiting throughout the IP cavity; instead, they gravitationally settle at the injection site. Ongoing studies are attempting to use fluid distension of the IP cavity to encourage dispersion; additional studies will use smaller  $^{29}\text{Si}$  nanoparticles for *in vivo* studies.

### 3.5 Initial Work in Tumor Models

Preliminary targeted studies in small animals utilized a *HeyA8* orthotopic ovarian cancer mouse model with the ESTA-1 functionalized silicon microparticles. Because of the difficulties with particle movement following intraperitoneal injection, these functionalized particles were directly injected into the tumor

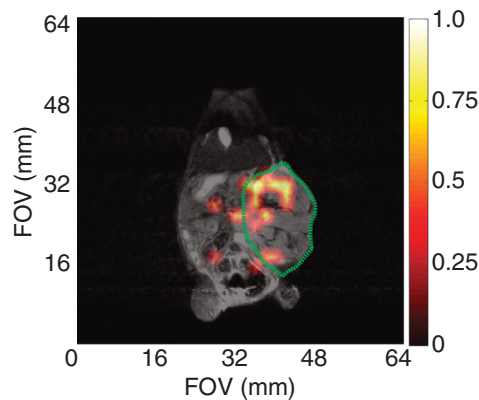


**Fig. 8** *In vivo*  $^{29}\text{Si}$  MRI of ESTA-1 functionalized  $2\ \mu\text{m}$  silicon particles (100 mg; dissolved in 400 ml PBS) directly injected into the tumor volume of an orthotopic ovarian cancer mouse (*HeyA8*). Tumor periphery outlined in green. Single image taken 20 min postinjection, showing the silicon particles retain their enhanced signal while in the tumor volume.  $^{29}\text{Si}$  imaging scan (color): 90 deg RARE imaging sequence, TR/TE: 59.9/1.8 ms, FOV:  $64 \times 64$  mm, resolution: 2 mm; single scan acquisition (scan time  $\sim 60$  ms), processed with 35% threshold to filter background. Coregistered with  $^1\text{H}$  imaging scan (grayscale): 90 deg RARE imaging sequence, coronal plane, TR/TE: 1927/9.5 ms, FOV:  $64 \times 64$  mm; resolution: 0.25 mm; four averages (scan time  $\sim 4$  min).

mass in 3 to 4 injections throughout the tumor volume. The hyperpolarized  $^{29}\text{Si}$  MRI signal was still present 20 min after injection (Fig. 8) and was predominately located within the tumor region. While this cannot be considered targeted imaging, the long-lasting  $^{29}\text{Si}$  signal inside the tumor boundary was an encouraging finding that will prompt future targeted imaging studies. The further development of sufficiently hyperpolarized nanoscale silicon particles should exhibit improved mobility and allow for true targeted imaging.

### 3.6 Potential for Prospective Clinical Translation

Given their biocompatibility and the nontoxic, nonionizing nature of both MRI and hyperpolarization, there is expected to be a low barrier to eventual clinical translation of HP silicon particles for MRI applications. The  $^{29}\text{Si}$  precession frequency is observable on most multinuclear MRI scanners; however, companies will need to develop and test suitable clinical-scale  $^{29}\text{Si}$  MR coils and optimize imaging sequences to efficiently use the long-lasting, enhanced signal. Dosing and toxicity studies will be required, and will likely benefit from a current clinical trial<sup>5</sup> that examines the role of silicon particles as drug delivery agents for treating pancreatic cancer. Also, the recent push of different hyperpolarized modalities into the clinic<sup>9</sup> may simplify many of the initial burdens of introducing a new HP contrast agent into human studies. In addition to targeting ovarian cancer, ESTA-1 functionalized silicon particles may be used for molecular imaging of other cancer systems that overexpress E-Selectin—including breast, prostate, colorectal, and pancreatic cancers.<sup>24</sup> Furthermore, silicon particles may also be developed as a platform technology to interrogate a number of disease systems (through conjugation of additional targeting moieties) for multiplexed diagnostics. Given the very long hyperpolarized relaxation times and ability to perform molecular targeting (as opposed to metabolic tracing), silicon particles have the potential to bridge the gap between hyperpolarized imaging and nanomedicine.

## 4 Conclusions

In this work, we demonstrate the hyperpolarization of a variety of different silicon particle sizes and surface chemistries. The larger microparticles provided the highest signal enhancements over the longest time durations, likely due to their polycrystalline/amorphous structure and smaller surface-to-volume ratio when compared to smaller particles. The addition of targeting groups to the particles' surface did not alter the hyperpolarization dynamics, as the free electrons necessary for DNP were endogenous to the particles. High field MR imaging was accomplished using phantoms and mouse models via a variety of particle administration methods. These results represent encouraging findings for applying hyperpolarized silicon particles as noninvasive molecular imaging agents. However, work is still needed; ongoing studies involve developing small, more physiologically relevant nanoparticles for *in vivo* imaging and continuing with the targeted imaging studies in orthotopic mouse models.

### Acknowledgments

Portions of this work previously appeared in Proc. SPIE Vol. 9417, 941702 (2015). The authors would like to thank Drs. M.C. Cassidy (TU-Delft), C. Marcus (U. of Copenhagen), D. Gorenstein (UTHSCH), and J. Bankson and M. Ramirez (MDACC) for helpful discussions, and Ms. L.

Bitner and Dr. D. Young (MDACC) for assistance with the animal studies. This work was funded by the MD Anderson Cancer Center Odyssey Postdoctoral Fellowship, NCI R25T CA057730/CA016672, DoD PC131680, MDACC Institutional Research Grants, MDACC Institutional Startup, NCI U54 CA151668, P50 CA083639, Leukemia and Brain SPORE Developmental Research Awards, NCI R21 CA185536, Gulf Coast Consortium, Blanton-Davis Ovarian Cancer Research Program Grant, CPRIT RP150701, and NCI Cancer Center Support Grant CA016672. Author contributions: NW, JH, NMZ, GL, DV, DM, RR, RP, AS, and PB designed the study. NW and JH conducted the hyperpolarization and imaging studies. NMZ, NW, and JH conducted the particle functionalization study. GL and DV provided ESTA-1. RR, RP, and AS provided the orthotopic mouse models. NW and JH processed the data and constructed the figures. NW, JH, and PB wrote the paper, and all authors contributed to the review and editing of the paper. The authors declare no competing financial interests.

## References

- E. Tasciotti et al., "Mesoporous silicon particles as a multistage delivery system for imaging and therapeutic applications," *Nat. Nanotechnol.* **3**, 151–157 (2008).
- J.-H. Park et al., "Biodegradable luminescent porous silicon nanoparticles for *in vivo* applications," *Nat. Mater.* **8**, 331–336 (2009).
- L. A. Osminkina et al., "Photoluminescent biocompatible silicon nanoparticles for cancer theranostic applications," *J. Biophotonics* **5**, 529–535 (2012).
- F. Erogbogbo et al., "Biocompatible luminescent silicon quantum dots for imaging of cancer cells," *ACS Nano* **2**, 873–878 (2008).
- H. A. Santos, "Porous silicon for biomedical applications," in *Woodhead Publishing Series in Biomaterials*, Woodhead Publishing, Cambridge, UK (2014).
- J. Kim et al., "Multifunctional uniform nanoparticles composed of a magnetite nanocrystal core and a mesoporous silica shell for magnetic resonance and fluorescence imaging and for drug delivery," *Angew. Chem.* **47**, 8438–8441 (2008).
- J. Ruiz-Cabello et al., "Fluorine (19F) MRS and MRI in biomedicine," *NMR Biomed.* **24**, 114–129 (2011).
- K. Golman et al., "Metabolic imaging by hyperpolarized 13C magnetic resonance imaging for *in vivo* tumor diagnosis," *Cancer Res.* **66**, 10855–10860 (2006).
- S. J. Nelson et al., "Metabolic imaging of patients with prostate cancer using hyperpolarized [1-13C]pyruvate," *Sci. Transl. Med.* **5**, 198ra108 (2013).
- S. B. Fain et al., "Functional lung imaging using hyperpolarized gas MRI," *J. Magn. Reson. Imaging* **25**, 910–923 (2007).
- T. M. Atkins et al., "Synthesis of long T1 silicon nanoparticles for hyperpolarized 29Si magnetic resonance imaging," *ACS Nano* **7**, 1609–1617 (2013).
- A. E. Dementyev, D. G. Cory, and C. Ramanathan, "Dynamic nuclear polarization in silicon microparticles," *Phys. Rev. Lett.* **100**, 127601 (2008).
- M. Cassidy et al., "In vivo magnetic resonance imaging of hyperpolarized silicon nanoparticles," *Nat. Nanotechnol.* **8**, 363–368 (2013).
- M. Cassidy et al., "Radical-free dynamic nuclear polarization using electronic defects in silicon," *Phys. Rev. B* **87**, 161306(R) (2013).
- J. W. Aptekar et al., "Silicon nanoparticles as hyperpolarized magnetic resonance imaging agents," *ACS Nano* **3**, 4003–4008 (2009).
- N. Whiting et al., "Real-time MRI-guided catheter tracking using hyperpolarized silicon particles," *Sci. Rep.* **5**, 12842 (2015).
- M. Lee et al., "Decay of nuclear hyperpolarization in silicon microparticles," *Phys. Rev. B* **84**, 035304 (2011).
- A. P. Mann et al., "Identification of thioaptamer ligand against e-selectin: potential application for inflamed vasculature targeting," *PlosOne* **5**, e13050 (2010).
- A. P. Mann et al., "E-selectin-targeted porous silicon particle for nanoparticle delivery to the bone marrow," *Adv. Mater.* **23**, H278–H282 (2011).
- A. P. Mann et al., "Thioaptamer conjugated liposomes for tumor vasculature targeting," *Oncotarget* **2**, 298–304 (2011).
- S. Kang et al., "Safety evaluation of intravenously administered monothiolated aptamer against E-selectin in mice," *Toxicol. Appl. Pharmacol.* **287**, 86–92 (2015).
- S. Kang et al., "Blocking the adhesion cascade at the pre-metastatic niche for prevention of breast cancer metastasis," *Mol. Ther.* **23**, 1044–1054 (2015).
- J. Mai et al., "Bone marrow endothelium-targeted therapeutics for metastatic breast cancer," *J. Controlled Release* **187**, 22–29 (2014).
- A. P. Mann and T. Tanaka, "E-selectin: its role in cancer and potential as a biomarker," *Transl. Med.* **S1**(2) (2011).

**Nicholas Whiting** earned his PhD in physical chemistry at Southern Illinois University Carbondale (2010) for work in the field of hyperpolarized noble gases. He continued this line of research as an NSF International Research fellow at the Sir Peter Mansfield Imaging Centre at the University of Nottingham, UK. As an Odyssey and NCI R25T fellow at MD Anderson Cancer Center, he is developing hyperpolarized silicon nanoparticles for targeted molecular imaging of different cancer systems.

**Jingzhe Hu** graduated with a BSE degree in biomedical engineering from Duke University. He is currently a PhD student in the Department of Bioengineering at Rice University and works on targeted MR imaging with hyperpolarized silicon particles in the Bhattacharya laboratory at UT MD Anderson Cancer Center.

**Niki M. Zacharias** earned her PhD in chemistry at California Institute of Technology. She went on to work in biotechnology at Neuron Pharmaceuticals and later became the Boswell fellow between Huntington Medical Research Institutes and California Institute of Technology. As the Boswell fellow, she began working in the new field of hyperpolarization and medical imaging. As a faculty member, she is using hyperpolarized imaging to monitor the efficacy of treatment and interrogate the metabolism of cancer.

**Ganesh L. R. Lokesh** earned his PhD in biochemistry and molecular virology at Indian Institute of Science, Bangalore for his work studying structure and assembly of icosahedral plant viruses. He continued his studies on structure and assembly of spherical animal viruses such as VEE at UTMB Galveston. He switched to the drug discovery field to screen and develop small molecules and DNA aptamers targeting cancer at the University of Texas Health Science Center, Houston.

**David E. Volk** earned his PhD in physical chemistry at North Dakota State University for his work studying Lewis acid-mediated organic chemical reaction mechanisms by NMR spectroscopy and quantum chemistry. He determined the NMR structures of DNA and proteins. His most recent work involves development of DNA aptamers targeting cancer at Duke University, University of Texas Medical Branch in Galveston, and University of Texas Health Science Center at Houston.

**David G. Menter** earned his PhD in biology at Wayne State University for studies in platelet and prostaglandin biology in cancer metastasis. He was awarded an NIH fellowship in genetics at MD Anderson Cancer Center. As a faculty member in the Department of Gastrointestinal Medical Oncology at MD Anderson, he is helping to understand aspirin acetylation, stem cell metabolism, and imaging of colorectal cancer using hyperpolarized imaging.

**Rajasha Rupaimoole** earned his PhD in biomedical sciences with a major in cancer biology at the Graduate School of Biomedical Sciences, UT Health Science Center, and UT MD Anderson Cancer Center, Houston (2015) for work studying delineating mechanisms by which miRNA biogenesis alterations occur in tumor microenvironments. As a postdoctoral fellow at Beth Israel Deaconess Medical Center and Harvard Medical School, he is developing better miRNA therapeutics against lung cancer.

**Rebecca Previs** earned her MD at the University of Virginia (2009) and completed her residency at Duke University Medical Center in

obstetrics/gynecology (2013). As a fellow in gynecologic oncology at MD Anderson Cancer Center, her interests include therapeutics and altered metabolism in gynecologic malignancies.

**Anil K. Sood** is a professor and vice chairman for Translational Research in the Department of Gynecologic Oncology at the University of Texas MD Anderson Cancer Center. He is also codirector of the Center for RNA Interference and Non-Coding RNA and Director of the Blanton-Davis Ovarian Cancer Research Program at MD Anderson. His main research interests include neuroendocrine effects on cancer metastasis, RNA interference-based therapeutics,

and the development of new strategies for targeting the tumor microenvironment.

**Pratip Bhattacharya** earned his PhD in chemistry at California Institute of Technology for studying the dynamics of electron transfer through DNA mismatches. He is currently an associate professor in the Department of Cancer Systems Imaging at the University of Texas MD Anderson Cancer. His research is focused on real-time metabolic and molecular imaging and studying metabolism in cancer systems employing hyperpolarization of small molecule and silicon nanoparticles as well as MRI and NMR spectroscopy.